Structured light sheet fluorescence microscopy based on four beam interference

Ming Lei, [1, 2] Andreas Zumbusch[1,*]

[1] *Department of Chemie, University of Konstanz, D-78457 Konstanz, Germany*
[2] *Permanent address: State Key Laboratory of Transient Optics and Photonics, Xi'an Institute of Optics and Precision Mechanics, Chinese Academy of Sciences, Xi'an 710119, China*
** andreas.zumbusch@uni-konstanz.de*

Abstract: A 3D structured light sheet microscope using a four-faceted symmetric pyramid is presented. The sample is illuminated by the resulting four beam interference field. This approach combines advantages of standing wave and structured illumination microscopy. Examples of micrographs of fluorescently labeled Chinese hamster ovary (CHO) cells as well as of the compound eyes of drosophila are shown and the optical sectioning ability of our system is demonstrated. The capabilities and the limitations of the scheme are discussed.

OCIS codes: (180.2520) Fluorescence microscopy; (260.3160) Interference.

References and links

1. J. Huisken, J. Swoger, F. Del Bene, J. Wittbrodt, and E. H. K. Stelzer, "Optical sectioning deep inside live embryos by selective plane illumination microscopy," Science **305**(5686), 1007–1009 (2004).
2. P. J. Keller, A. D. Schmidt, J. Wittbrodt, and E. H. K. Stelzer, "Reconstruction of zebrafish early embryonic development by scanned light sheet microscopy," Science **322**(5904), 1065–1069 (2008).
3. J. A. Buytaert, and J. J. Dirckx, "Design and quantitative resolution measurements of an optical virtual sectioning three-dimensional imaging technique for biomedical specimens, featuring two-micrometer slicing resolution," J. Biomed. Opt. **12**(1), 014039 (2007).
4. E. Fuchs, J. S. Jaffe, R. A. Long, and F. Azam, "Thin laser light sheet microscope for microbial oceanography," Opt. Express **10**(2), 145–154 (2002).
5. H. U. Dodt, U. Leischner, A. Schierloh, N. Jährling, C. P. Mauch, K. Deininger, J. M. Deussing, M. Eder, W. Zieglgänsberger, and K. Becker, "Ultramicroscopy: three-dimensional visualization of neuronal networks in the whole mouse brain," Nat. Methods **4**(4), 331–336 (2007).
6. T. F. Holekamp, D. Turaga, and T. E. Holy, "Fast three-dimensional fluorescence imaging of activity in neural populations by objective-coupled planar illumination microscopy," Neuron **57**(5), 661–672 (2008).
7. P. J. Keller, and E. H. K. Stelzer, "Quantitative in vivo imaging of entire embryos with Digital Scanned Laser Light Sheet Fluorescence Microscopy," Curr. Opin. Neurobiol. **18**(6), 624–632 (2008).
8. J. Swoger, P. Verveer, K. Greger, J. Huisken, and E. H. K. Stelzer, "Multi-view image fusion improves resolution in three-dimensional microscopy," Opt. Express **15**(13), 8029–8042 (2007).
9. P. J. Verveer, J. Swoger, F. Pampaloni, K. Greger, M. Marcello, and E. H. K. Stelzer, "High-resolution three-dimensional imaging of large specimens with light sheet-based microscopy," Nat. Methods **4**(4), 311–313 (2007).
10. B. Bailey, D. L. Farkas, D. L. Taylor, and F. Lanni, "Enhancement of axial resolution in fluorescence microscopy by standing-wave excitation," Nature **366**(6450), 44–48 (1993).
11. F. Lanni, and B. Bailey, "Standing-wave excitation for fluorescence microscopy," Trends Cell Biol. **4**(7), 262–265 (1994).
12. R. Freimann, S. Pentz, and H. Hörler, "Development of a standing-wave fluorescence microscope with high nodal plane flatness," J. Microsc. **187**(3), 193–200 (1997).
13. M. A. A. Neil, R. Juskaitis, and T. Wilson, "Method of obtaining optical sectioning by using structured light in a conventional microscope," Opt. Lett. **22**(24), 1905–1907 (1997).
14. M. A. A. Neil, R. Juskaitis, and T. Wilson, "Real time 3D fluorescence microscopy by two beam interference illumination," Opt. Commun. **153**(1-3), 1–4 (1998).
15. D. Karadaglić, and T. Wilson, "Image formation in structured illumination wide-field fluorescence microscopy," Micron **39**(7), 808–818 (2008).
16. M. G. L. Gustafsson, "Surpassing the lateral resolution limit by a factor of two using structured illumination microscopy," J. Microsc. **198**(2), 82–87 (2000).
17. M. G. L. Gustafsson, "Nonlinear structured-illumination microscopy: wide-field fluorescence imaging with theoretically unlimited resolution," Proc. Natl. Acad. Sci. U.S.A. **102**(37), 13081–13086 (2005).

#132099 - $15.00 USD Received 21 Jul 2010; revised 13 Aug 2010; accepted 16 Aug 2010; published 25 Aug 2010

18. M. G. L. Gustafsson, L. Shao, P. M. Carlton, C. J. R. Wang, I. N. Golubovskaya, W. Z. Cande, D. A. Agard, and J. W. Sedat, "Three-dimensional resolution doubling in wide-field fluorescence microscopy by structured illumination," Biophys. J. **94**(12), 4957–4970 (2008).
19. L. Schermelleh, P. M. Carlton, S. Haase, L. Shao, L. Winoto, P. Kner, B. Burke, M. C. Cardoso, D. A. Agard, M. G. L. Gustafsson, H. Leonhardt, and J. W. Sedat, "Subdiffraction multicolor imaging of the nuclear periphery with 3D structured illumination microscopy," Science **320**(5881), 1332–1336 (2008).
20. P. Kner, B. B. Chhun, E. R. Griffis, L. Winoto, and M. G. L. Gustafsson, "Super-resolution video microscopy of live cells by structured illumination," Nat. Methods **6**(5), 339–342 (2009).
21. T. Breuninger, K. Greger, and E. H. K. Stelzer, "Lateral modulation boosts image quality in single plane illumination fluorescence microscopy," Opt. Lett. **32**(13), 1938–1940 (2007).
22. M. Lei, B. L. Yao, and R. A. Rupp, "Structuring by multi-beam interference using symmetric pyramids," Opt. Express **14**(12), 5803–5811 (2006).
23. S. Hell, and E. H. K. Stelzer, "Properties of a 4Pi confocal fluorescence microscope," J. Opt. Soc. Am. A **9**(12), 2159–2166 (1992).
24. M. G. L. Gustafsson, D. A. Agard, and J. W. Sedat, "I^5M: 3D widefield light microscopy with better than 100 nm axial resolution," J. Microsc. **195**(1), 10–16 (1999).
25. L. Shao, B. Isaac, S. Uzawa, D. A. Agard, J. W. Sedat, and M. G. L. Gustafsson, "I^5S: wide-field light microscopy with 100-nm-scale resolution in three dimensions," Biophys. J. **94**(12), 4971–4983 (2008).
26. E. G. Reynaud, U. Kržič, K. Greger, and E. H. K. Stelzer, "Light sheet-based fluorescence microscopy: more dimensions, more photons, and less photodamage," HFSP J **2**(5), 266–275 (2008).

1. Introduction

Wide-field fluorescence microscopy techniques with axial section capability have recently met a lot of interest, since they combine high sensitivity down to the single molecule detection limit, short image acquisition times, and high 3D spatial resolution. The main approaches are light sheet based fluorescence microscopy (LSFM), standing wave excitation fluorescence microscopy (SWFM), and structured illumination microscopy.

LSFM techniques include variants such as Single Plane Illumination Microscopy (SPIM) [1], digital scanned laser light sheet fluorescence Microscopy (DSLM) [2], orthogonal Plane Fluorescence Optical Sectioning (OPFOS) [3], thin laser light sheet microscope (TLSM) [4], ultramicroscopy [5], and objective-coupled planar illumination microscopy(OCPI) [6]. Their common feature sample illumination with a thin light sheet, such that fluorescence is only excited in the portion which is actually observed. This is equivalent to optical sectioning, but generates less photo-damage outside the illuminated sheet plane, since specimens are exposed to less light energy than in confocal and two-photon fluorescence microscopes [7]. Commonly, a cylindrical lens is used in LSFM to focus the Gaussian beam to a thin light sheet. The focused light sheet then always has a divergence angle which is inversely proportional to the thickness of the sheet such that the intensity distribution inside the focused light-sheet is not uniform but has a Gaussian profile. The axial resolution of light sheet microscopy is dominated by the thickness of the light sheet. While thinner sheets lead to better axial resolution, they are also accompanied by a more pronounced non-uniform intensity distribution. The non-uniform illumination problem can be solved by rotating the specimen within the light sheet. Multi-view information can be combined into a single image by image processing algorithm [8], but this limits the image acquisition speed and introduces vibrations. Dodt et al. used two sided illumination to get more uniform illumination and higher imaging speed [5]. Like this, however, only a minor improvement in the axial resolution compared to standard wide field microscopy is achievable. Deconvolution algorithms can be used to increase the axial resolution of LSFM, but this approach is time-consuming [5, 9] and requires extensive computing resources.

In a different approach to depth resolved wide field microscopy, Bailey et al. [10, 11] introduced standing wave excitation (SWFM). SWFM can be viewed as a kind of multi-layer light sheet geometry. Fluorescence is excited in a series of parallel antinodal planes. Different from the single light sheets formed by the cylindrical lens, the intensity distribution is uniform inside each antinodes plane and varies rapidly in the axial direction. This leads to an improved axial resolution of up to 50 nm. However, this technique is most powerful when the thickness of the sample is comparable to the wavelength of light and just one or two antinodal planes lie within it. Otherwise several planes are illuminated simultaneously and their separation is difficult and will give a strong background [12].

#132099 - $15.00 USD Received 21 Jul 2010; revised 13 Aug 2010; accepted 16 Aug 2010; published 25 Aug 2010

This problem is not present using structured illumination, which was introduced by Neil [13] to wide field fluorescence microscopy as a means to discriminate against out-of-focus background and to get higher axial resolution [14, 15]. The idea is based on the zero spatial frequency being the only component of an image which is not attenuated with defocussing. Projecting a single spatial frequency fringe pattern onto the sample, the microscope will then image the grid pattern efficiently only on those parts of the sample which are in focus. Simple processing of three spatially modulated wide-field images permits an optically sectioned image to be extracted in real-time. The axial resolution of a structured illumination microscope can be as good as that of a confocal microscope. There have been numerous attempts to exploit structured illumination in microscopy to achieve different goals. Notably, Gustafsson et al. [16–20] used basically the same principle to get subdiffraction resolution, whereas Breuninger et al. also combined LSFM with structured illumination to improve the axial resolution when imaging strongly scattering sample [21].

In this paper, we present a 3D structured light sheet microscope which combines the advantages of standing wave microscopy and structured illumination microscopy. A four-faceted symmetric pyramid is used to generate a four beam interference field with the same periodicity in both lateral and axial direction. The sample is illuminated by a series of parallel antinodal planes, which is analogous to the standing wave microscopy. However, the light intensity inside each antinodal plane is not uniform but has the periodic distribution as found in structured illumination microscopy. By using the same image processing method used as Neil [13], the out of focus background excited simultaneously by the other antinodal planes can be suppressed. According to our calculation, the axial resolution of our system is slightly improved over the common structured illumination with fringe projection or grid projection geometry. The optical sectioning capability of the method is demonstrated by imaging two different biological samples.

2. Theory

Earlier, we have reported the generation of 2D and 3D optical structures by using rotationally symmetric pyramids [22]. The four-faceted pyramid is a wave-front division optical element. As Fig. 1(a) shows, a collimated beam incident on the base of the pyramid is deviated cylindrically toward the optical axis due to refraction. After the pyramid, four refracted rays overlap and interfere, resulting in a 3D interference lattice with the same periodicity in both lateral and axial direction, as is shown in Fig. 1(b)

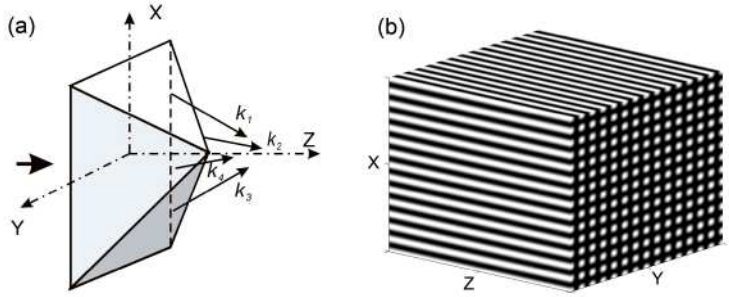

Fig. 1. 4 beams interference by a four-faceted symmetric pyramid (a) and the resulting interference lattice (b)

Figure 2 shows the planar geometrical scheme of a collimated beam passing through a glass pyramid. The periodicity of the interference lattice can be written as $\Delta=\lambda/2\sin\theta$, where λ is the wavelength and θ is half of the beam crossing angle. The extension of the resulting interference zone can be estimated by $Z_{max} \approx w_0 / \tan(\theta)$, where w_0 denotes the radius of the beam. Considering the light transmittance, the open angle γ is usually designed to be very small (we used a pyramid with $\gamma=7°$). To a good approximation, the divergence angle $\theta \approx$(n

#132099 - $15.00 USD Received 21 Jul 2010; revised 13 Aug 2010; accepted 16 Aug 2010; published 25 Aug 2010

−1) γ, where n is the refractive index of the glass pyramid. In our experiment, w_0 is 1.5 mm, γ is 7°, and n is 1.5, such that we obtain Z_{max} ≈24.5mm.

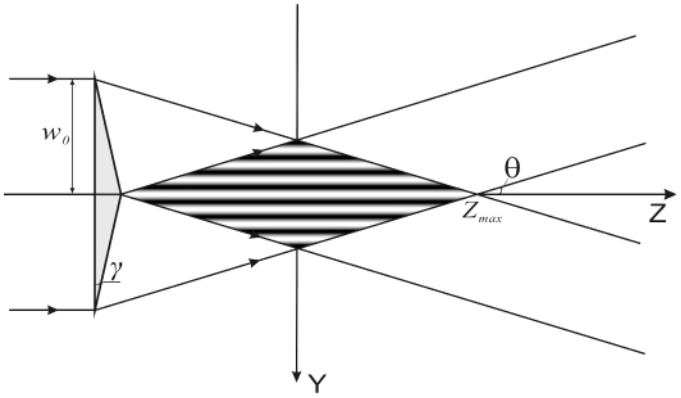

Fig. 2. Plane geometrical scheme of a collimated beam passing through a glass pyramid

The sample needs to be placed inside the interference zone defined by Z_{max}. In many cases this will mean that the available space is too small in order to allow the fixation of objectives and sample stage. To solve this problem, we build a telescope behind the pyramid by lens L_1 and L_2 and move the interference zone far away from the optics. Figure 3 illustrates the geometrical arrangement and parameters of the optical path. Based on the Gaussian formula of geometrical optics, it is not difficult to derive the following equations:

$$
\begin{aligned}
Z_{\max} &= \frac{h-(f_1+f_2)(\tan\theta_1+h/f_1)}{\tan(-\theta_2)} \\
Z_{\min} &= \frac{h-(f_1+f_2)(\tan\theta_1+h/f_1)}{\tan(-\theta_2)} - \frac{f_2 w_0}{f_1\tan(-\theta_2)} \\
\tan(-\theta_2) &= \tan\theta_1 + \frac{h}{f_1} + \frac{h-(f_1+f_2)(\tan\theta_1+h/f_1)}{f_2} \\
h &= w_0 - d_1\tan\theta_1 \\
\theta_1 &= (n-1)\gamma
\end{aligned}
\qquad (1)
$$

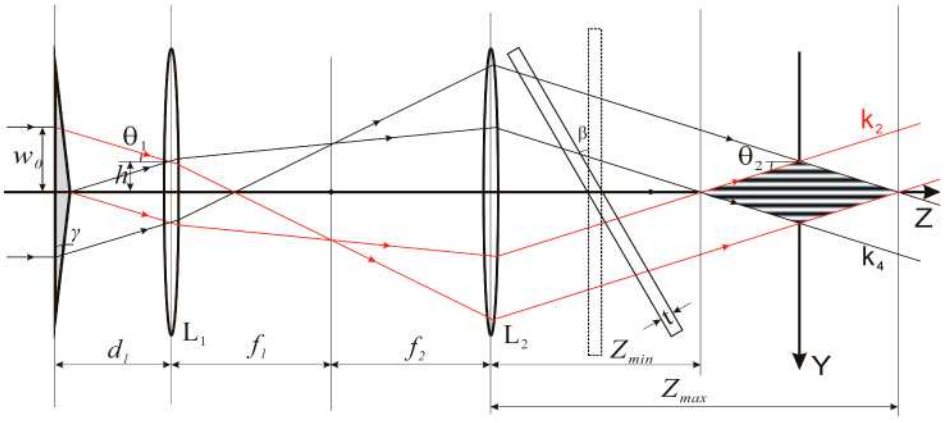

Fig. 3. Plane geometrical arrangement and parameters of a collimating beam passing through a pyramid and a pair of lenses.

#132099 - $15.00 USD Received 21 Jul 2010; revised 13 Aug 2010; accepted 16 Aug 2010; published 25 Aug 2010

In our setup, f_1=125 mm, f_2=50 mm are the focal lengths of L_1 and L_2, d_1=5mm. Substituting these parameters into the Eq. (1) results in Z_{max}=77mm, Z_{min}=73mm. Under these conditions we can get an interference zone with a length of 4 mm and 73 mm away from L_2. Another advantage of this improved geometry is that according to Eq. (2), the final beam crossing angle θ_2 is adjustable by changing the zoom ratio of the telescope formed by L_1 and L_2. Thus we can get different periodicities Δ of the structured light field in Fig. 1(b).

$$\Delta = \lambda / 2n \sin\theta_2, \text{ while } \quad \tan(\theta_2) = \frac{f_1 \tan((n-1)\gamma)}{f_2} \tag{2}$$

In order to obtain the three raw images with three spatial positions, we use a glass platelet behind L_2 to change the phase difference δ between k_2 and k_4. The phase difference δ can be written as:

$$\delta = \frac{2\pi}{\lambda}\left(\frac{nt}{\cos(\beta+\theta_2)} - \frac{nt}{\cos(\beta-\theta_2)}\right) \tag{3}$$

Where n is the refractive index of the glass platelet, and t is its thickness. According to Eq. (3), for small rotation angles β, the phase difference δ is directly proportional to β. Thus by rotating the plate glass, the interference pattern can be moved laterally and three images with a phase difference of δ=120° between any two images can be recorded. As is shown in Fig. 4,

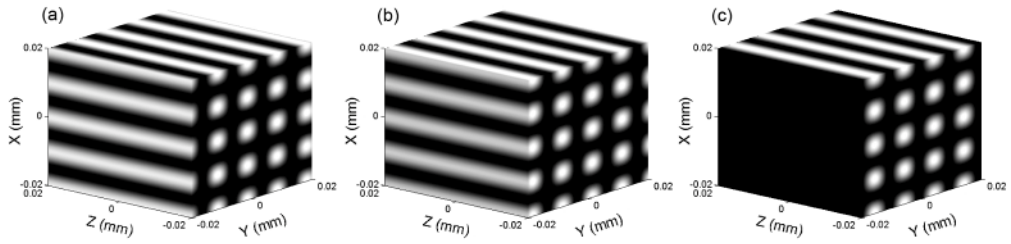

Fig. 4. Moving the interference pattern laterally by changing the phase difference δ. (a) δ=0°, (b) δ=120°, (c) δ=240°. (Media 1)

3. Experimental setup

Figure 5 shows the experimental layout of our structured light sheets microscopy system. A diode-pumped Solid-State laser (VERDI V18, Coherent Inc., USA) working at a wavelength of 532 nm, after beam collimating, is deviated into 4 beams by the pyramid prism. The four beams pass through lens L_1 and L_2 and then interfere to a 3D structured pattern. In order to get a high contrast interference field the beams must be S polarized. The sample is fixed on a sample stage and illuminated by the 3D structured field. A plate glass is fixed on a rotation stage to control the phase difference between k_2 and k_4. The fluorescence signal was detected perpendicular to the excitation beam path by using a 40x objective (HCX PL Apo, NA 0.85, Leica, Germany) or a long working distance 20x objective(EO M Plan HR, NA 0.6, 13mm working distance, Edmund Optics, USA). A USB CCD camera (DMK 41BU02, 1280*960 pixels, The Imaging Source Europe GmbH, Germany) is employed to capture the 2D fluorescence image. A long-pass filter (LP02-568RS, AHF Analysentechnik AG, Germany) is put in front of the camera to block the excitation laser beams. The maximum laser powers on the sample used in our experiments are 50 mW. During the recording process, three images ($I_{0°}$, $I_{120°}$, $I_{240°}$) with a phase shift of δ=120° between any two images are acquired for each plane in the stack of images The recording time varies between 0.05 and 0.1 s for one image. Each image triple is then processed according to Neil [13, 14]

$$I_x(y,z) = \sqrt{[(I_0 - I_{120})^2 + (I_{120} - I_{240})^2 + (I_{240} - I_0)^2)]/2} \tag{4}$$

#132099 - $15.00 USD Received 21 Jul 2010; revised 13 Aug 2010; accepted 16 Aug 2010; published 25 Aug 2010

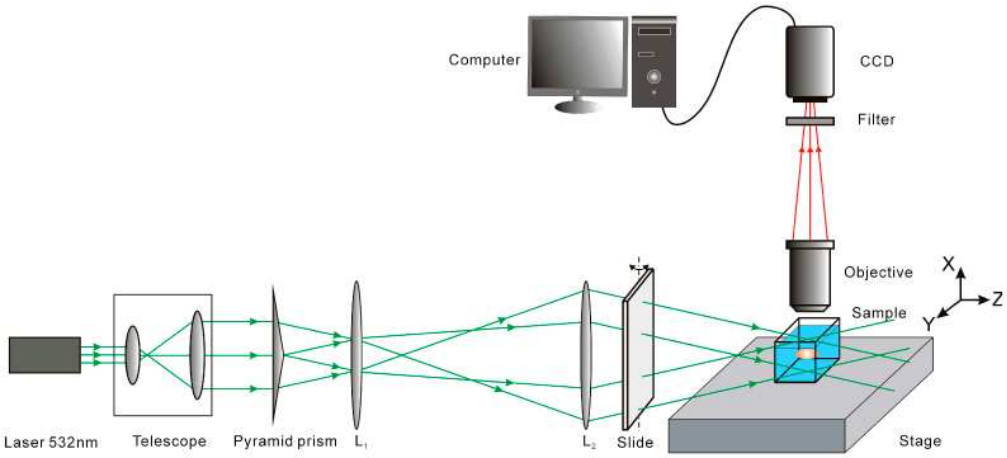

Fig. 5. Schematic of the experimental system.

3.2 Materials

The wild-type Chinese Hamster Ovary clone cells (Toronto strain) were grown in Eagle's minimum essential medium (Gibco) supplemented with 8% heat inactivated foetal bovine serum (Gibco), 0.584 g/L L-glutamine (Gibco), 3.5 g/L D-glucose (Sigma), 2.95 g/L tryptose-phosphate (Sigma), 100 U/mL penicillin (Gibco), 100 mg/L streptomycin (Gibco) and BME vitamins (Sigma).

The penetration of propidium iodide (PI) was performed by electroporation. The electric field generator (GHT Unipolar 2000V, Betatech, Toulouse, France) delivers square-wave electric pulses. Two stainless-steel plate parallel electrodes (length = 10 mm, inter-electrode distance = 4 mm), connected to the voltage generator, give a uniform electric field. Cells in suspension (106 cells) were centrifuged for 5 min at 120 x g, resuspended in 100 µL PI-containing pulsation buffer (i.e. 100µL PI in 10 mM phosphate pH 7.4, 1 mM MgCl2, 250 mM sucrose), and put between the 4 mm plate electrodes. The electric field parameters were 10 pulses of 5 ms length, 0.7 kV/cm intensity and 1 Hz frequency at room temperature (RT).

Drosophilae were raised in the standard medium (100 ml, containing 91.8 ml of water, 11.8 g of sugar beet syrup, 1.08 g of yeast, 0.406 g of agar, 9.4 g of cornmeal and 0.24 ml of propionic acid) at 25°C, 65% relative humidity under a 12/12 light/dark cycle. All experimental drosophilae were female and at the age of from 14 to 21 days. The head was separated from the body by using micro-scissors (Fine Science Tools Inc. Europe).

4. Results and discussion

This section demonstrates the optical sectioning abilities of our method. In structured illumination microscopy, the normalized spatial frequency $\tilde{\nu} = \lambda / (\Delta * NA)$ is introduced in order to describe the axial response of the system, where λ is the wavelength and Δ is the spatial periodicity of the projected structure. The $\tilde{\nu} = 0$ case corresponds to the conventional wide field microscope, while the maximum sectioning strength corresponds to a normalized spatial frequency $\tilde{\nu} = 1$ [15]. In our experimental setup the period of the illuminating fringes was adjusted to $\Delta = 1.75$ µm. With the objective used, either a 40x objective or a long working distance 20x objective this corresponds to $\tilde{\nu} = 0.5071$ and $\tilde{\nu} = 0.3579$, respectively.

Figure 6 shows a series images of the thick volume structure of the compound eyes of drosophila with the 20X, 0.6 NA, long working distance objective. The distance between the successive series of images in the figure is 10µm. In the left column we show the optically sectioned images, whereas in the right column of the images the corresponding conventional wide field images are shown. This figure demonstrates optical sectioning, as well as improved contrast in comparison to the conventional image.

#132099 - $15.00 USD Received 21 Jul 2010; revised 13 Aug 2010; accepted 16 Aug 2010; published 25 Aug 2010

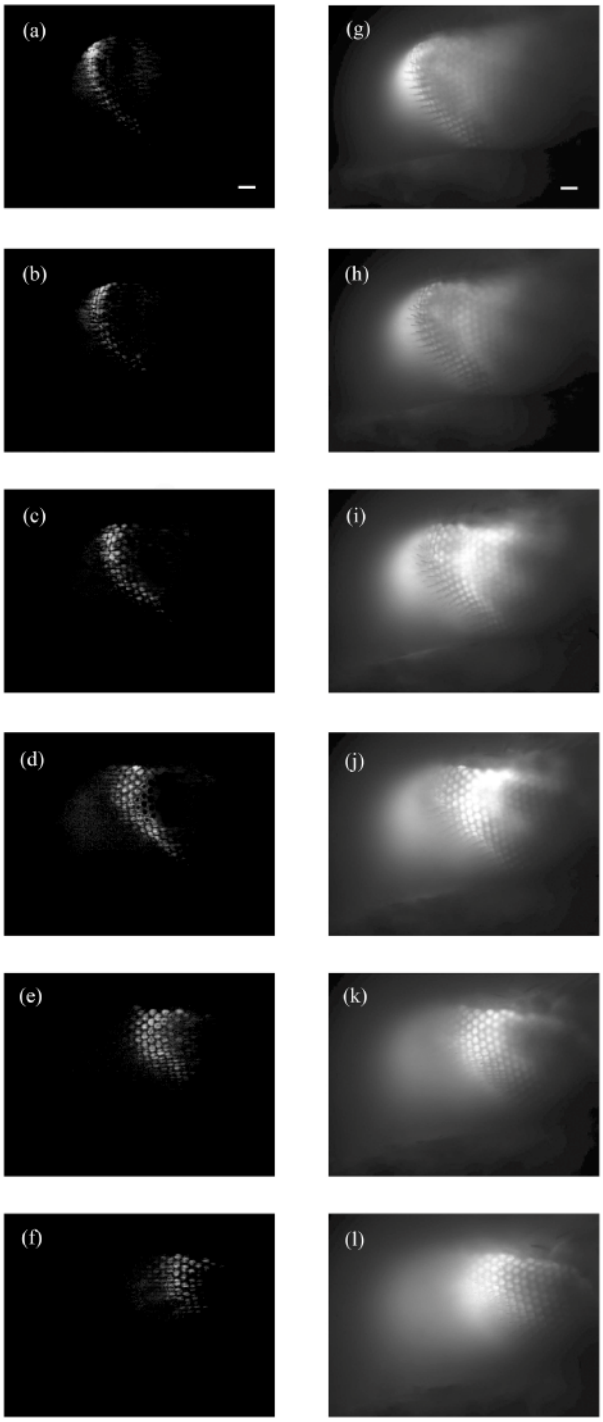

Fig. 6. Example of a through-focus series of images of compound eyes of drosophila, scale bar is 20 μm, the distance between planes is 10 μm.

Our method also can be used to observe single cells in vivo. In Fig. 7 we show an image series of propidium iodide (PI) labeled Chinese hamster ovary (CHO) cells with the 40X, 0.85 NA objective. The distance between the successive series of images in the figure is 1.75μm.

#132099 - $15.00 USD Received 21 Jul 2010; revised 13 Aug 2010; accepted 16 Aug 2010; published 25 Aug 2010

In the left column we show the optically sectioned images, whereas in the right column of the images the corresponding conventional wide field images are shown.

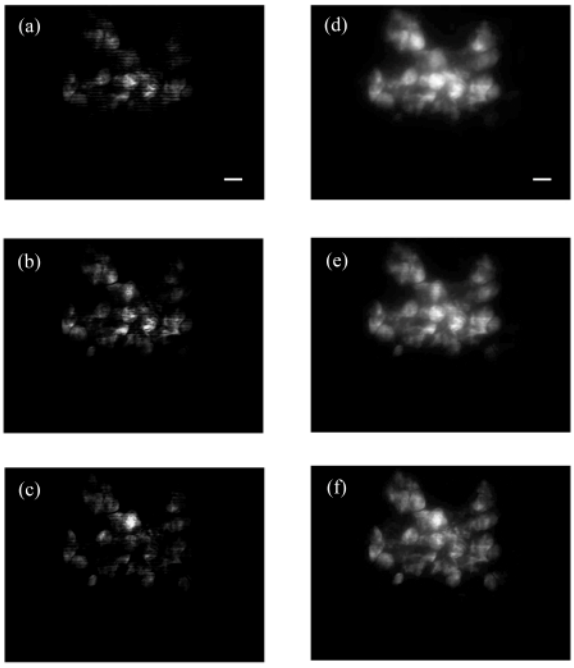

Fig. 7. Example of a through-focus series of images of propidium iodide labeled Chinese hamster ovary cells, scale bar is 10 μm, the distance between planes is 1.75 μm.

Structured illumination microscopy has an axial resolution which is comparable to confocal microscopy. There are two methods of obtaining structured illumination: fringe projection [13] and grid projection [14]. Compared to the grid projection geometry, fringe projection uses two coherent beams which interfere to get the structured illumination. This has the advantages of a simple setup and reduced aberrations, but comes with the price of poorer axial resolution. In the fringe projection case, the fringe pattern is uniform in depth along the optic axis, while in the grid projection approach, the structured pattern is formed by imaging a physical grid onto the specimen. The signal is detected with the same objective, hence the fringe pattern is attenuated with defocusing resulting in an improvement of the axial resolution of the grid projection system [15]. Our four beam interference geometry combines the advantages of both methods.

As a combination of standing wave microscopy and structured illumination microscopy, the intensity structure of the four beam interference geometry has both a varying axial and a varying lateral intensity distribution. The axial point spread function (PSF) of our system can be calculated by multiplying the x axial intensity distribution of illumination (as shown in Fig. 1(b)) with the PSF of the detection. The periodicity of the axial intensity of the four beams interfering field is adjustable by changing the beam crossing angle θ and the axial resolution of our system. It can be smaller than the structured illumination with fringe and grid projection geometry. We compared the axial response of these three kinds of structured illumination geometry by the method described in [15], as is shown in Fig. 8 by using the 20x NA 0.6 objective. The FWHM of the axial response of our system can be smaller than 1 micron, which is less than the axial period (1.75μm) of the four beams interference lattice. The out of focus background can be completely suppressed. While our approach cannot reduce photo-bleaching to the degree as encountered in LSFM, the light intensity at the maxima of the four beams interfering field is 16 times that of the incident beams. This implies

#132099 - $15.00 USD Received 21 Jul 2010; revised 13 Aug 2010; accepted 16 Aug 2010; published 25 Aug 2010

that four times less total incident power can be used compared to fringe projection and 16 times less compared to grid projection structured illumination geometries.

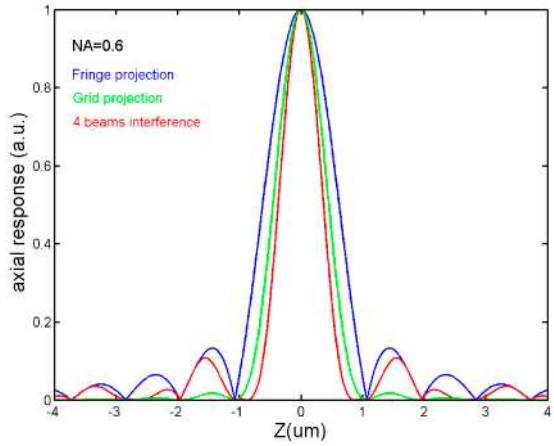

Fig. 8. Simulated axial response of structured illumination with fringe and grid projection and our 4 beams interference geometry

Our structured light sheet microscopy and other recent techniques, such as SWFM [10–12], 4Pi confocal [23], I^nM [24] or I^5S [25], are all based on interference. The phase of the interference is determined by the optical path length difference between the interferential branches. For maximum interference contrast, this difference should be small compared to the coherence length of the light, and the ideal condition is zero path length difference. Splitting a laser beam into several components of equal intensity usually requires a complicated experimental setup and suffers from low stability. Using a diffractive beam splitter one can easily get a multi-beam with more components, but at the disadvantage of low transmittance and of laser mode degradation. The solution presented here is based on pyramids made from optical glass. They have the benefit of good stability, high damage threshold and high transmission, and can be used with all kinds of CW and pulsed lasers. The zero path length difference can be easily matched.

It should be noted that the interference effects can be disturbed by refractive index mismatch between the sample and surrounding media. This problem can be diminished by sample preparation protocols or by deconvolution algorithms. It has been pointed out that sample preparation is an important issue with LSFM techniques [26]. In our case the difficulties are smaller, since long working distance objectives are used. The simplest approach then is to put the specimen into a chamber with four glass windows and filled with refractive index matched solution or to fix it between two thin glass cover slides. Actually, sometimes it is difficult to perfectly eliminate the phase error over the entire image (1280*960), however, within a sub-area of the image, this error is small enough to be neglected.

5. Conclusion

In conclusion we have presented a new approach to implementing a 3D structured light sheet microscopy geometry with an increased axial resolution by using a four-faceted symmetric pyramid. Examples of micrographs of fluorescently labeled Chinese hamster ovary (CHO) cells as well as of the compound eyes of drosophila are given and the optical sectioning ability of our system is demonstrated. Our technique is simple to implement and combines advantages of both standing wave and structured illumination microscopy.

#132099 - $15.00 USD Received 21 Jul 2010; revised 13 Aug 2010; accepted 16 Aug 2010; published 25 Aug 2010

Acknowledgments

This work was supported by the Center for Applied Photonics (CAP) at the University of Konstanz, the German Federal Ministry of Education and Research in the framework of its "Technologie-Initiative Molekulare Bildgebung - MoBiTech" and the Chinese Academy of Sciences (CAS)/State Administration of Foreign Experts Affairs of China (SAFEA) International Partnership Program for Creative Research Teams. We thank Christelle Rosazza for help in the preparation of the cell samples and Shouwen Ma and Prof. Giovanni Galizia for the Drosophila samples.

#132099 - $15.00 USD Received 21 Jul 2010; revised 13 Aug 2010; accepted 16 Aug 2010; published 25 Aug 2010